Hepatic NF-κB essential modulator deficiency prevents obesity-induced insulin resistance but synergizes with high-fat feeding in tumorigenesis

F. Thomas Wunderlich*, Tom Luedde[†‡], Stephan Singer[§], Marc Schmidt-Supprian[¶], Julia Baumgartl*, Peter Schirmacher[§], Manolis Pasparakis[†‡], and Jens C. Brüning*[‖]

*Department of Mouse Genetics and Metabolism, Institute for Genetics, University of Cologne and Center of Molecular Medicine Cologne, D-50674 Cologne, Germany; [†]Department of Mouse Genetics and Inflammation, Institute for Genetics, University of Cologne, D-50674 Cologne, Germany; [‡]European Molecular Biology Laboratory Mouse Biology Unit, I-00016 Monterodondo, Italy; [§]Institute of Pathology, University of Heidelberg, D-69120 Heidelberg, Germany; and [¶]CBR Institute for Biomedical Research, Harvard Medical School, 200 Longwood Avenue, Boston, MA 02115

Communicated by C. Ronald Kahn, Harvard Medical School, Boston, MA, September 7, 2007 (received for review April 4, 2007)

Development of obesity-associated insulin resistance and diabetes mellitus type 2 has been linked to activation of proinflammatory pathways in the liver, leading to impaired insulin signal transduction. To further define the role of hepatic NF-κB activation in this process, we have analyzed glucose metabolism in mice with liver-specific inactivation of the NF-κB essential modulator gene (NEMO$^{L\text{-}KO}$ mice) exposed to a high-fat diet (HFD). These animals are protected from the development of obesity-associated insulin resistance, highlighting the importance of hepatic NF-κB activation in this context. However, hepatic NEMO deficiency synergizes with HFD in the development of liver steatosis as a consequence of decreased peroxisome proliferator-activated receptor (PPAR-α) and increased PPAR-γ expression. Steatosis interacts with increased inflammation, causing elevated apoptosis in the livers of these mice under HFD. These changes result in liver tumorigenesis of NEMO$^{L\text{-}KO}$ mice under normal diet, a process that is largely aggravated when these mice are exposed to HFD. These data directly demonstrate the interaction of hepatic inflammation, dietary composition, and metabolism in the development of liver tumorigenesis.

insulin sensitivity | spontaneous hepatic carcinoma | steatosis | hepatic NEMO deficiency

Excessive weight gain is associated with a chronic inflammatory state in white adipose tissue that releases proinflammatory cytokines such as TNF and IL-6 into circulation (1). While adipocytes have also been demonstrated to exhibit increased expression of proinflammatory cytokines in obesity (1), more recent studies have revealed that increased macrophage infiltration of white adipose tissue contributes to the proinflammatory state under conditions of obesity (2). These cytokines inhibit insulin action in classical insulin target tissues such as skeletal muscle, liver, and adipose cells, thereby resulting in alterations of glucose homeostasis (3). More recently, TNF-stimulated activation of the JNK and NF-κB signaling pathways has been demonstrated to inhibit insulin action in a tissue-specific manner (3–5). With respect to NF-κB signaling, TNF binding induces activation of the IKK-1 and -2 kinases that are released from a multiproteincomplex containing the regulatory subunit NF-κB essential modulator (NEMO), thereby mediating phosphorylation and subsequent proteasomal degradation of I-κBs liberating the transcription factor NF-κB.

In addition to predisposing to insulin resistance and diabetes, obesity also represents a major risk factor for the development of the malignant neoplasias (4–8). It has been clearly demonstrated that metabolic syndrome is a key factor leading to sequential development of hepatic steatosis, steatohepatitis, hepatic fibrosis, cirrhosis, and finally increased frequency of hepatocellular carcinoma (HCC) (10). Thus, steatohepatitis represents a key feature of this particular tumor entity. Recent work has also demonstrated that the NF-κB signaling pathway plays a crucial role in the development of malignant neoplasias of the liver. Inactivation of the IKK-2 gene resulted in increased tumor formation in a mouse model of chemically induced hepatocarcinogenesis (11). On the other hand, NF-κB inhibition in the liver by transgenic expression of an I-κBα superrepressor led to a reduced number of tumors in the Mdr-2-deficient model of liver cancer, which develops tumors because of chronic cholangitis (12). Moreover, mice lacking NEMO in liver parenchymal cells (NEMO$^{L\text{-}KO}$) spontaneously develop chronic hepatitis characterized by increased apoptosis and reactive proliferation of hepatocytes, inflammation, liver steatosis, dysplasia, and activation of liver progenitor cells, resulting in the development of hepatocellular carcinoma (13). Therefore, NF-κB signaling represents a key mechanism both in the regulation of obesity-associated insulin resistance and hepatocellular carcinogenesis.

Results

Liver-Specific NEMO Inactivation. To further define the role of NF-κB activation in the regulation of metabolic and inflammatory pathways in the liver, we used mice lacking NEMO specifically in liver parenchymal cells (NEMO$^{L\text{-}KO}$), generated by crossing NEMO$^{FL/FL}$ mice (14) with ALFP-Cre mice (15). Southern blot and immunoblot analysis revealed efficient recombination of the loxP-flanked NEMO allele exclusively in hepatocytes of NEMO$^{L\text{-}KO}$ mice without altering expression of hepatic IKK1 and IKK2 [supporting information (SI) Fig. 5 *a–d*].

To directly address the impact of abolished NEMO expression and subsequent lack of IKK activation on obesity-induced insulin resistance, groups of control and NEMO$^{L\text{-}KO}$ mice were analyzed both under normal chow diet (NCD) and high-fat diet (HFD). There was no significant difference in body weight of control and NEMO$^{L\text{-}KO}$ mice under NCD (Fig. 1*a*). While control mice significantly gained weight upon exposure of HFD, weight gain was greatly attenuated in NEMO$^{L\text{-}KO}$ mice on a HFD (Fig. 1*a*). To directly address whether hepatic NEMO deficiency protects from the development of obesity in NEMO$^{L\text{-}KO}$ mice exposed to HFD, we next determined white adipose tissue mass in these animals. Similar to body weight, epigonadal fat-pad weight was not significantly different between control and NEMO$^{L\text{-}KO}$ mice exposed to NCD (Fig. 1*b*). In contrast, there was significant

Author contributions: F.T.W. and J.C.B. designed research; F.T.W., S.S., and J.B. performed research; T.L., M.S.-S., and M.P. contributed new reagents/analytic tools; F.T.W. and P.S. analyzed data; and F.T.W. and J.C.B. wrote the paper.

The authors declare no conflict of interest.

[‖]To whom correspondence should be addressed. E-mail: jens.bruening@uni-koeln.de.

This article contains supporting information online at www.pnas.org/cgi/content/full/0707849104/DC1.

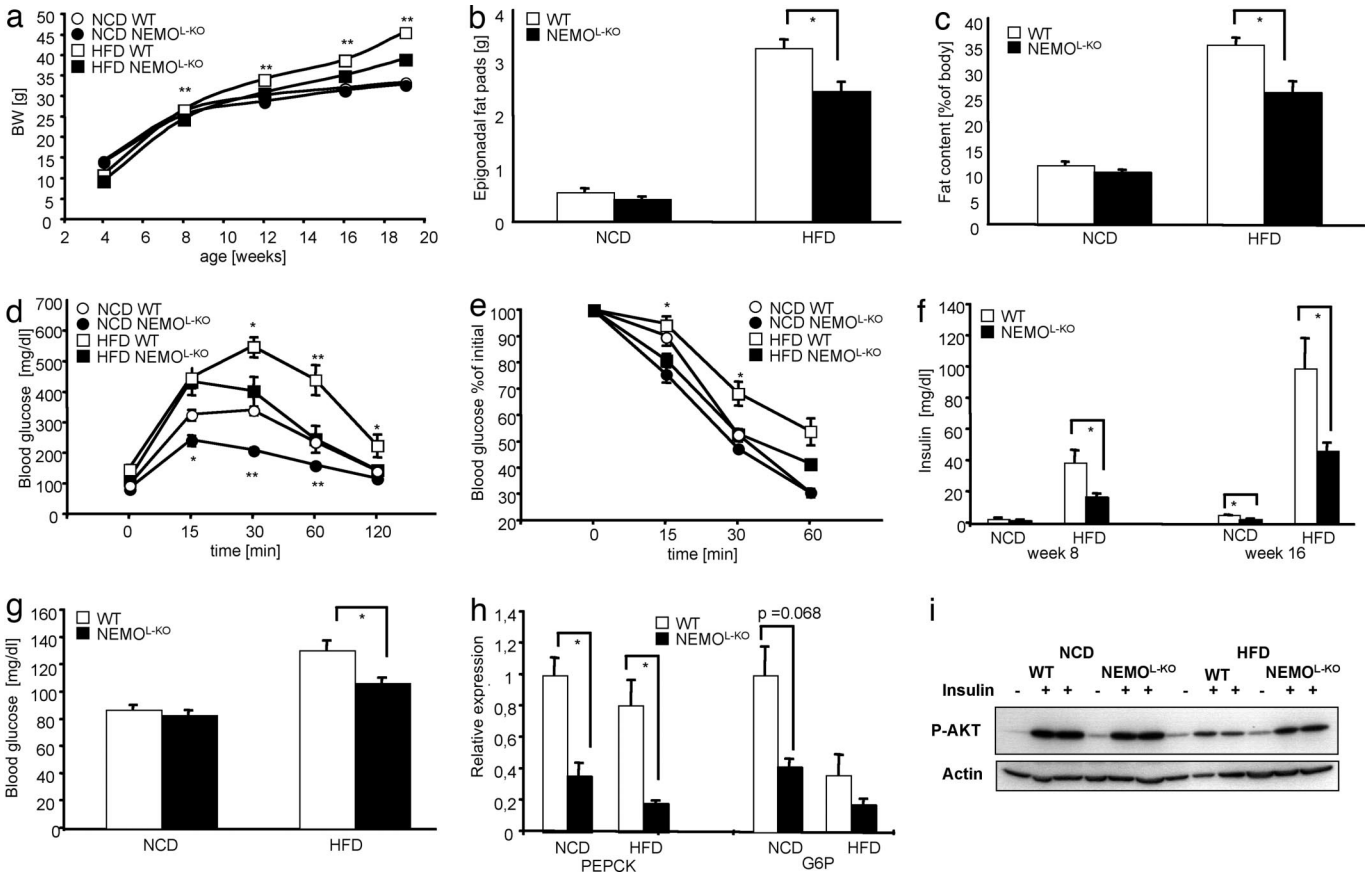

Fig. 1. Metabolic phenotype of NEMO$^{L\text{-}KO}$ mice on NCD and HFD. (*a*) Body weights of WT mice on a NCD (open circles) and a HFD (open squares) were compared with NEMO$^{L\text{-}KO}$ mice on NCD (filled circles) and HFD (filled squares). The weight of nine mice was determined weekly for each genotype. (*b*) The epigonadal fat pad weight of WT (white bars) and NEMO$^{L\text{-}KO}$ (black bars) on NCD and on HFD was measured at week 19 ($n = 9$ per genotype). (*c*) Body compositions of WT (white bars) and NEMO$^{L\text{-}KO}$ (black bars) on NCD and on HFD were determined by using a Brucker minespec ($n = 7$ per genotype). (*d*) Glucose tolerance tests of WT mice on NCD (open circles), on HFD (open squares) and of NEMO$^{L\text{-}KO}$ mice on NCD (filled circles) and on HFD (filled squares) were performed at week 12 ($n = 9$ per genotype). (*e*) Insulin tolerance tests of mice with the indicated genotypes were performed at week 13 ($n = 9$ per genotype). (*f*) Serum insulin levels were determined by ELISA from sera of mice with the indicated genotypes at 8 and 16 weeks of age ($n = 9$ per genotype). (*g*) Fasted blood glucose was evaluated at week 13 ($n = 9$ per genotype). (*h*) Relative expression of gluconeogenic enzymes PEPCK and G6P were determined by real-time PCR from liver samples of the indicated genotypes ($n = 8$ per genotype) using TaqMan Assay. (*i*) Representative insulin signaling of mice with the indicated genotypes by using Western blot analysis with the indicated antibodies. Mice were injected into the vena cava with 125 μl of 40 units/ml insulin upon anesthetization. Values are mean ± SEM. *, $P \leq 0.05$; **, $P \leq 0.001$ vs. control.

reduction in epigonadal fat-pad weight of NEMO$^{L\text{-}KO}$ mice compared with control animals when exposed to HFD (Fig. 1*b*). Consistently, analysis of body composition in these four groups of mice by NMR spectroscopy revealed a significantly reduced gain of fat mass in NEMO$^{L\text{-}KO}$ mice only after HFD feeding (Fig. 1*c*). Nevertheless, also NEMO$^{L\text{-}KO}$ mice still exhibited a clear >3-fold increase in white adipose tissue mass upon exposure to HFD (Fig. 1 *b* and *c*). Thus, high-fat feeding still results in obesity in NEMO$^{L\text{-}KO}$ mice.

Improved Glucose Metabolism in NEMO$^{L\text{-}KO}$ Mice. We next determined glucose homeostasis in these animals. Glucose tolerance tests revealed a significant improvement of glucose tolerance in NEMO$^{L\text{-}KO}$ mice compared with control mice under NCD (Fig. 1*d*). Although exposure to HFD resulted in severe impairment of glucose tolerance in control animals, lack of hepatocellular NEMO resulted in improved glucose tolerance (Fig. 1*d*). Consistently, liver-specific disruption of NEMO completely prevented the occurrence of insulin resistance otherwise associated with high-fat feeding as assessed by insulin tolerance tests (Fig. 1*e*, SI Fig. 6). We next determined plasma insulin concentrations in control and NEMO$^{L\text{-}KO}$ mice as another indirect measure of insulin resistance. This analysis revealed already in 8-week-old mice a significant increase in circulating plasma insulin concentrations of control mice when exposed to HFD (Fig. 1*f*). Although there was no significant difference in circulating plasma insulin concentrations in control and NEMO$^{L\text{-}KO}$ mice at this age under NCD, hepatic NEMO deficiency reduced plasma insulin concentrations in NEMO$^{L\text{-}KO}$ mice compared with controls under HFD (Fig. 1*f*). Consistent with improved glucose tolerance of NEMO$^{L\text{-}KO}$ mice under NCD, also plasma insulin concentrations were significantly reduced in these mice at the age of 16 weeks (Fig. 1*f*). Even more strikingly, whereas exposure to HFD led to a >20-fold increase of circulating plasma insulin concentrations of control mice at 16 weeks of age, plasma insulin concentrations were lowered by >60% in NEMO$^{L\text{-}KO}$ mice (Fig. 1*f*). Similarly, the obesity-associated increase in fasting blood glucose concentrations was significantly reduced in NEMO$^{L\text{-}KO}$ mice (Fig. 1*g*). Accordingly, NEMO$^{L\text{-}KO}$ mice exhibited a >80% reduction in the expression of key enzymes of gluconeogenesis such as phosphoenolpyruvate carboxykinase (PEPCK) and glucose-6-phosphatase (G6P) (Fig. 1*h*). Analysis of insulin-stimulated AKT phosphorylation in liver revealed a significant improvement of insulin sensitivity in the livers of

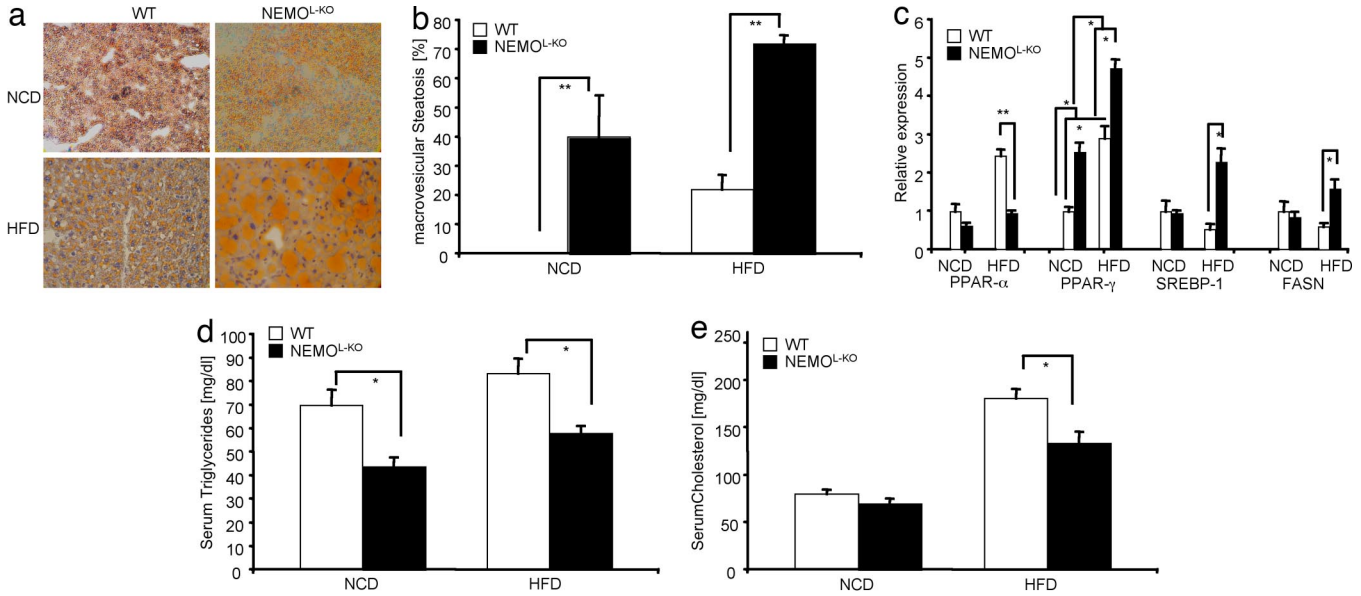

Fig. 2. Macrovesicular steatosis in livers of NEMO^{L-KO} mice. (*a*) Representative Sudan staining from liver sections of control and NEMO^{L-KO} mice on NCD and HFD at 5 months of age. Sections were counterstained with hematoxylin. (*b*) Percentage of macrovesicular lipid accumulations in lipid containing hepatocytes. (*c*) Relative expression of the indicated genes from the different genotypes was performed by real-time PCR by using TaqMan Assay ($n = 8$ per genotype). Values are mean ± SEM. *, $P \leq 0.05$; **, $P \leq 0.001$ vs. control. (*d*) Triglyceride and (*e*) cholesterol levels from sera of control and NEMO^{L-KO} mice on NCD and HFD at week 16 were determined by a diagnostic laboratory using standard techniques ($n = 16$ per genotype).

NEMO^{L-KO} mice, whereas HFD feeding resulted in severe insulin resistance in control mice (Fig. 1*i*). Taken together, these analyses revealed a striking improvement of glucose homeostasis in NEMO^{L-KO} mice, demonstrating almost complete protection from the occurrence of obesity-associated insulin resistance, glucose intolerance, and fasting hyperglycemia as a consequence of inhibiting NF-κB activation in liver parenchymal cells.

Aggravated Liver Steatosis in NEMO^{L-KO} Mice. Feeding a HFD to mice results in increased accumulation of lipids in the liver and is an accepted model for hepatic steatosis (16). Therefore, we analyzed the effect of HFD on steatosis in the different groups of mice. To detect lipid accumulations in the liver, we performed Sudan stainings of liver sections of control and NEMO^{L-KO} mice on either NCD or HFD (Fig. 2*a*). Even NEMO^{L-KO} mice on NCD exhibited a low degree of steatosis, but this was further aggravated by feeding a HFD. Although the percentage of hepatocytes with lipid deposits was similar in controls compared with NEMO^{L-KO} mice on a HFD (data not shown), the lipid accumulations in hepatocytes of NEMO^{L-KO} mice were overall macrovesicular, whereas control HFD mice exhibited mainly microvesicular steatosis (Fig. 2 *a* and *b*). Taken together, these data indicate that HFD and hepatic NEMO deficiency synergize to increase steatosis.

To analyze the mechanism responsible for lipid accumulation in hepatocytes of NEMO^{L-KO} mice, we performed real-time PCR analyses to monitor the expression levels of the peroxisome proliferator-activated receptor (PPAR)-α, the key transcriptional regulator of β-oxidation, and for essential regulators of lipid synthesis, such as PPAR-γ and sterol regulatory element-binding protein (SREBP)-1 as well as their transcriptional target gene fatty acid synthase (FASN) (17–19). As previously described, high-fat feeding of control mice results in increased PPAR-α transcription as a compensatory response to activate transcription of genes required for β-oxidation to dispense unphysiological lipid stores in the liver (20) (Fig. 2*c*). However, the liver of NEMO^{L-KO} mice on a HFD failed to up-regulate PPAR-α mRNA (Fig. 2*c*). Therefore, we conclude that the inability of the NEMO-deficient liver to up-regulate PPAR-α expression contributes to inhibition of β-oxidation and thus to aggravated storage of triglycerides in hepatocytes. In addition, the key transcription factors activating *de novo* lipid synthesis, PPAR-γ and SREBP-1, are up-regulated in livers of NEMO^{L-KO} mice on HFD, leading to significantly elevated expression of FASN (Fig. 2*c*). Taken together, the reduced β-oxidation and increased lipogenesis in livers of NEMO^{L-KO} mice on HFD result in macrovesicular steatosis with the concomitant inability to efflux excessive lipids and cholesterol to the bloodstream, as demonstrated by significantly reduced plasma concentrations of triglycerides and cholesterol in these mice (Fig. 2 *d* and *e*).

HFD Enhances Apoptosis in Livers of NEMO^{L-KO} Mice. The progression from steatosis to steatohepatitis correlates with infiltration of activated macrophages in the liver (21). Therefore, we directly determined whether HFD results in increased liver inflammation in NEMO^{L-KO} mice by examining the inflammatory infiltration of liver in the different groups of mice. F4/80 staining of macrophages revealed massive macrophage infiltration into liver tissues of NEMO^{L-KO} mice on NCD as well as on HFD, whereas livers of control mice did not exhibit a significant infiltration (Fig. 3*a*). Consistent with a higher degree of inflammation in livers of NEMO^{L-KO} mice on HFD compared with NCD and to control mice, there was significantly increased hepatic expression of macrophage derived inflammatory cytokines and chemokines such as TNF and MCP-1 in these mice (Fig. 3*b*). However, although feeding a HFD to WT mice resulted in macrophage infiltration into white adipose tissue leading to the local expression of cytokines and chemokines such as TNF, MCP-1, and IL-6 in white adipose tissue, this response to HFD was reduced in NEMO^{L-KO} mice (SI Fig. 7*a*). Both Western blot and PCR analyses of white adipose tissue confirmed the lack of NEMO inactivation in white adipose tissue of NEMO^{L-KO} mice (SI Fig. 7 *b* and *c*). These data argue for a differential tissue distribution of macrophages as a consequence of hepatic NEMO deficiency. One potential explanation for reduced white adipose tissue inflammation might be an overriding inflammatory reac-

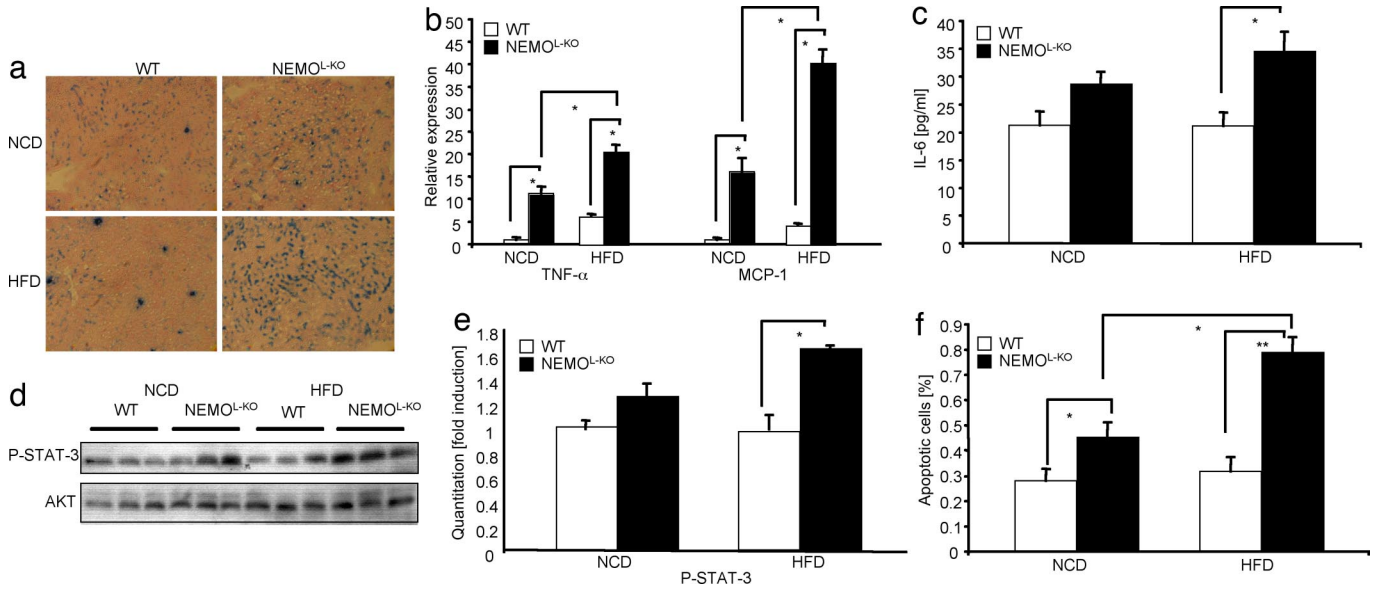

Fig. 3. Massive macrophage infiltration into livers of NEMO^{L-KO} mice leads to up-regulation of proinflammatory cytokines, induction of cell death and compensatory proliferation. (*a*) Immunohistochemistry of liver cryostat sections of control and NEMO^{L-KO} mice using F4/80 antibody to detect infiltrating macrophages. (*b*) Relative expression of MCP-1 and TNF-α in livers of control and NEMO^{L-KO} mice on NCD and HFD was determined by real-time PCR using TaqMan Assay ($n = 8$ per genotype). (*c*) Evaluation of IL-6 levels was performed by ELISA from sera of control and NEMO^{L-KO} mice on NCD and HFD at 16 weeks of age. (*d*) Representative Western blots of liver protein lysates from control and NEMO^{L-KO} mice on NCD and HFD using the indicated antibodies ($n = 3$ per genotype). (*e*) Quantitation of P-STAT-3 intensities from Western blots shown in *d* by using Quantity one software. (*f*) Determination of apoptosis by TUNEL staining of livers of control and NEMO^{L-KO} mice was expressed as percentage of total cells. TUNEL-stained liver sections were counterstained with DAPI and from five exemplary sections (see SI Fig. 7) for each value DAPI as well as TUNEL-positive cells were counted ($n = 5$ per genotype). Values are mean ± SEM. *, $P \leq 0.05$; **, $P \leq 0.001$ vs. control.

tion in livers of NEMO^{L-KO} mice, thus predominantly recruiting myeloid cells to this site. Furthermore, NEMO^{L-KO} mice showed significantly increased serum IL-6 levels compared with controls when mice were fed with HFD but not NCD (Fig. 3*c*), whereas serum levels for TNF and MCP-1 were unchanged in mice on a HFD (SI Fig. 6 *b* and *c*). Thus, high-fat feeding synergizes with hepatic NEMO deficiency to cause a greatly exaggerated inflammatory response in the liver of NEMO^{L-KO} mice.

To address whether increased hepatic expression of proinflammatory cytokines also translates into enhanced cytokine action on a molecular level in the liver of NEMO^{L-KO} mice, we assessed the activation of key pathways that are activated by cytokines and implicated in the regulation of liver cell growth and survival (22, 23). This analysis revealed enhanced activation of signals initiated by cytokine receptors of the IL-6 family, because NEMO^{L-KO} mice exposed to HFD exhibited a significant increase in tyrosine phosphorylation of STAT-3 compared with controls receiving the same diet (Fig. 3 *d* and *e*). Thus, consistent with significantly increased serum concentration of IL-6, signaling downstream of the IL-6 receptor appeared to be enhanced in liver of NEMO^{L-KO} mice exposed to HFD.

To investigate whether feeding of HFD aggravates not only inflammation but also hepatocellular apoptosis, we next directly determined the percentage of apoptotic cells in liver of the different groups of mice by TUNEL assay (SI Fig. 8). Quantitation of apoptotic cells revealed an increase in hepatic apoptosis in NEMO^{L-KO} mice compared with controls on both diets but strikingly also a significant increase in apoptosis in NEMO^{L-KO} mice on HFD compared with NEMO^{L-KO} mice on NCD (Fig. 3*f*). Thus, high-fat feeding causes increased inflammation and hepatocyte apoptosis in the liver of NEMO^{L-KO} mice. At this point, one cannot distinguish whether these events occur independently or whether increased hepatocyte apoptosis leads to inflammation or vice versa.

NEMO Deficiency Synergizes with HFD in Liver Tumorigenesis. To evaluate the effect of HFD on the development of liver tumors in this model, we compared the development of tumors in 5-month-old NEMO^{L-KO} mice fed with either NCD or HFD (Fig. 4*a*). Strikingly, quantitative assessment of macroscopically visible lesions demonstrated a 10-fold increase both in the number of small (<2 mm) and large nodules (>2 mm) in NEMO^{L-KO} mice fed with HFD compared with NCD (Fig. 4*b*). Livers of control mice exhibited no macroscopically visible tumors both under NCD and HFD (Fig. 4*a*). Subsequent histological examination of liver tissue confirmed the absence of tumors in control mice both under normal chow diet and HFD (Fig. 4 *c* and *d*). Again, there was a dramatic 4-fold increase in tumorigenesis in NEMO^{L-KO} mice when exposed to HFD (Fig. 4*e*).

To further characterize tumor development in NEMO^{L-KO} mice, multiple tumors were dissected from livers of NEMO^{L-KO} mice and protein levels of NEMO, phosphorylated I-κBα and I-κBα were examined (SI Fig. 9*a*). These hepatic tumors in younger NEMO^{L-KO} mice contained variable but intermediate protein levels of NEMO and exhibited elevated phosphorylation of IκBα (SI Fig. 9*b*). These findings offer the possibilities that either infiltrating activated macrophages or inefficient or still ongoing recombination from the ALFP-Cre transgene are accounting for the increased phosphorylation of IκBα and the intermediate levels of NEMO in dissected tumors, because we have previously shown that tumors in older mice exhibit a high degree of NEMO deficiency (13). To directly address the nature of cells exhibiting increased IκBα phosphorylation, we performed immunohistochemical analyses of liver tissue from control and NEMO^{L-KO} mice using anti P-IκBgα antibody (SI Fig. 9*c*). This analysis revealed on the one hand a striking accumulation of P-IκBα-positive cells surrounding the tumors in livers of NEMO^{L-KO} mice and on the other hand predominantly locating at the endothelium of the hepatic blood vessels and ducts. Taken together, inactivation of NEMO specifically in liver

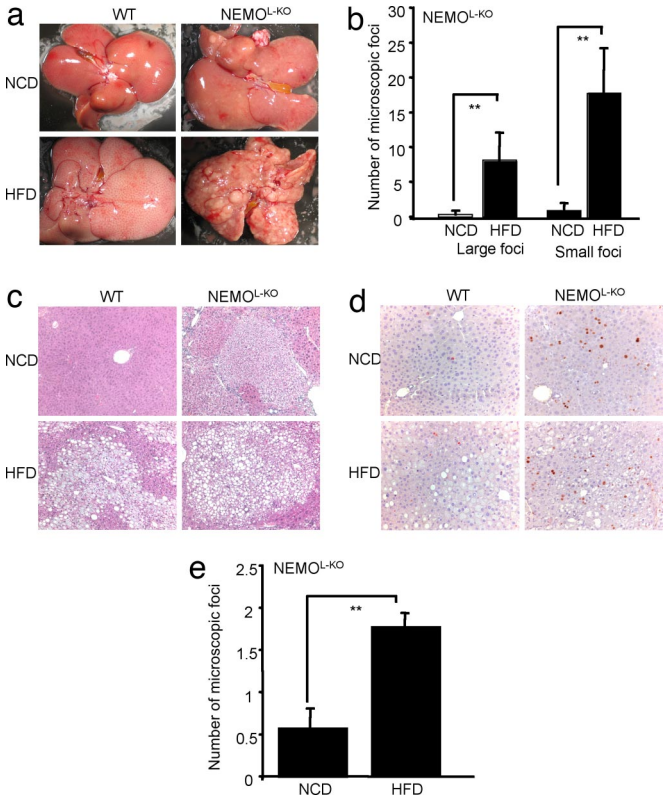

Fig. 4. HFD drastically elevates spontaneous tumorigenesis in livers of NEMO^{L-KO} mice. (*a*) Exemplary demonstration of *ex situ* isolated livers of control and NEMO^{L-KO} mice on NCD and HFD. (*b*) Macroscopic quantitation of large (>2-mm) and small (≤2-mm) foci of NEMO^{L-KO} mice on NCD and HFD (n = 5 per genotype) at week 19. (*c*) Representative paraffin sections of control and tumorigenic liver tissue from NEMO^{L-KO} mice on NCD and HFD. (*d*) Determination of proliferating cells in livers of control and NEMO^{L-KO} mice either on NCD or HFD was performed by immunohistochemistry using Ki-67 antibody. (*e*) Microscopic quantitation of foci in livers of NEMO^{L-KO} mice on a NCD and a HFD (n = 5 per genotype). A value of 1 expresses one to three foci/lobule, whereas a value of 2 represents more than three foci/lobule. Values are mean ± SEM. *, $P \leq 0.05$; **, $P \leq 0.001$ vs. control.

parenchymal cells results in liver tumorigenesis, which is dramatically increased when the mice are exposed to HFD.

Discussion

Here, we demonstrate that blocking hepatic NF-κB by disrupting NEMO in liver parenchymal cells prevents HFD-induced insulin resistance, but high-fat feeding results in exacerbated inflammation, apoptosis, and steatosis in NEMO^{L-KO} mice, ultimately leading to increased tumorigenesis in these mice. Because obesity has recently been recognized as a chronic inflammatory state, where increased circulating concentrations of proinflammatory cytokines impair insulin action in metabolically relevant tissues such as skeletal muscle and liver, interfering with cytokine signaling has opened a promising avenue for the treatment of obesity-associated insulin resistance. Along this line, improved glucose metabolism in NEMO^{L-KO} is consistent with recent reports that both hepatocyte-restricted inactivation of IKK-2 (21) and hepatic overexpression of the I-κB-superrepressor result in improved glucose tolerance and down-regulation of key enzymes of gluconeogenesis (8). These studies are also consistent with previous findings indicating that salicylate-mediated inhibition of IKK activity improves obesity-associated attenuation of insulin resistance by down-regulation of inhibitory serine phosphorylation of insulin receptor substrate proteins and assign the liver a key role in this process (25).

However, the metabolic improvement resulting from NEMO ablation in hepatocytes is much more striking than that described for hepatocyte-specific IKK-2 deficiency. This presumably results from the fact that inactivation of IKK-2 leads only to a partial block of NF-κB signaling, whereas NEMO deficiency completely abolishes TNF's ability to activate the NF-κB pathway (26). Thus, these studies consistently highlight the importance for activation of the hepatic IKK pathway in the development of obesity-associated insulin resistance.

Moreover, hepatic NEMO deficiency and HFD result in increased IL-6 concentrations and subsequent enhancement of hepatic STAT-3-phosphorylation. This may also contribute to reduced expression of key enzymes of gluconeogenesis in liver of NEMO^{L-KO} mice, because it was recently demonstrated that disruption of STAT-3 specifically in hepatocytes increases gluconeogenesis (27). This pathway appears to be involved in insulin's ability to act via the central nervous system to suppress hepatic glucose production, because i.c.v. insulin stimulates IL-6 expression in Kupffer cells, which in turn activates STAT-3 in hepatocytes to suppress G6P and PEPCK expression (28). Thus, increased IL-6 release as a result of hepatic NEMO deficiency may activate this pathway.

Additionally, reduced PPAR-α expression present in NEMO^{L-KO} mice may also further contribute to improved insulin sensitivity, because PPAR-α-deficient mice also exhibit improved glucose tolerance under both NCD and HFD (20).

Surprisingly, we observed strongly aggravated tumorigenesis in livers of NEMO^{L-KO} mice when feeding HFD. Our analysis revealed a 4- to 10-fold increase in spontaneous tumorigenesis in NEMO^{L-KO} mice on a HFD compared with NEMO^{L-KO} mice on NCD, whereas no tumors were observed in control mice both under NCD and HFD. Apparently, this synergism depends on the interplay among inflammation, steatosis, and programmed cell death, which is caused by a complete block of inducible NF-κB signaling in liver parenchymal cells. Hepatocytes with impaired NF-κB signaling are rendered sensitive to TNF-induced apoptosis (14). Although it remains unclear what the source for TNF is in mice under a normal diet, increased concentrations of TNF have been demonstrated to result from macrophage activation in white adipose tissue upon exposure to HFD (2). Indeed, we could demonstrate elevated apoptosis in livers of NEMO^{L-KO} mice under HFD. These data are consistent with enhanced chemically induced liver carcinogenesis in mice with liver-specific disruption of IKK-2, where sustained JNK activity and apoptosis have been demonstrated to induce compensatory proliferation of neighboring hepatocytes (11). An important difference in our current model is that it does not depend on chemical induction of carcinogenesis but synergizes with high-fat feeding. Because a high-fat-containing diet represents a common feature in the Western lifestyle, particularly in obese patients suffering from type 2 diabetes mellitus, the synergistic action of high-fat feeding, liver steatosis, and NF-κB inhibition in tumorigenesis has to be considered when one is intending to treat obese patients with NF-κB-inhibiting agents to improve glucose metabolism.

Moreover, the present study provides previously undescribed insight into the interaction of HFD with liver inflammation, steatosis, and tumorigenesis. The expression of the key transcription factor for β-oxidation PPAR-α is down-regulated in NEMO^{L-KO} mice exposed to HFD concomitantly with an increased expression of genes involved in fatty acid synthesis leading to lipid accumulations in hepatocytes and thus to macrovesicular steatosis. Potentially impaired PPAR-α sensing in livers of NEMO^{L-KO} mice on a HFD accounts for this effect, because PPAR-α-deficient mice exhibit macrovesicular steatosis with increased expression of PPAR-γ and SREBP-1 (20). Con-

cordantly with a previous report (29), we speculate that PPAR-α expression is influenced by TNF also manifested by the existence of several consensus sequences for NF-κB and AP-1 in close vicinity upstream of the PPAR-α gene. Further investigation of the molecular interaction between NF-κB and PPAR in hepatic steatosis and carcinogenesis may help to develop therapeutic approaches for the treatment of hepatic tumors associated with metabolic diseases and obesity.

Materials and Methods

Animal Care. Care of all animals was within institutional animal care committee guidelines. All animal procedures were conducted in compliance with protocols and approved by local government authorities (Bezirksregierung Köln, Cologne, Germany). Animals were fed either normal chow (Teklad Global Rodent 2018; Harlan) containing 53.5% carbohydrates, 18.5% protein, and 5.5% fat (12% of calories from fat), or a HFD (C1057; Altromin) containing 32.7% carbohydrates, 20% protein, and 35.5% fat (55.2% of calories from fat) starting from 4 weeks of age. Body weight was measured once per week.

Generation of NEMO$^{L\text{-}KO}$ Mice. All mice used in this study were pure C57/BL6 background. NEMO$^{FL/FL}$ female mice were mated with male ALFP-Cre heterozygous mice to obtain male NEMO$^{L\text{-}KO}$ and control animals. Genotyping for ALFP-Cre was performed by PCR by using primers 5Cre (5′-ACG-AGT-GAT-GAG-GTT-CGC-A-3′) and 3Cre (5′-ATG-TTT-AGC-TGG-CCC-AAA-TGT-3′). NEMO$^{FL/FL}$ genotyping was performed as described (11).

Physiological Characterization. Glucose and insulin tolerance tests were performed on animals that had been fasted for 16 h. Animals were injected with either 2 g/kg body weight of glucose or 0.75 units/kg body weight of human regular insulin (Novo Nordisk) into the peritoneal cavity. Blood glucose concentrations were determined by using an automated glucose monitor (GlucoMen) for the indicated time points.

Cytokine Determinations. Levels for insulin, IL-6, MCP-1, and TNF were examined by ELISA (Chrystal Chem, BD Bioscience PharMingen) according to the manufacturer's protocol. Serum levels of triglycerides and cholesterol were determined in a diagnostic laboratory by standard procedures.

Gene Expression Analysis. Quantitative expression for mRNAs PEPCK, G6P, MCP-1, TNF-α, PPAR-α, PPAR-γ, SREBP-1, and FASN were determined by using whole-liver RNA isolated by TRIzol (Invitrogen). RNA was reversely transcribed with Euroscript Kit (Eurogentec) and amplified by using TaqMan universal master mix, NO AmpErase UNG with TaqMan Assay on demand kits (Applied Bioscience). Relative expression of mRNAs was determined by using standard curves based on hepatic cDNA, and samples were adjusted for total RNA content by either TATA-box-binding protein or glucuronidase β quantitative PCR. Calculations were performed by a comparative cycle threshold (Ct) method: starting copy number of test samples was determined in comparison with the known copy number of the calibrator sample (ddCt). The relative gene copy number was calculated as 2^{-ddCt}. Quantitative PCR was performed on an ABI PRISM 7900 Sequence Detector (Applied Bioscience). Assays were linear $>$4 orders of magnitudes. Quantitative expression for mRNAs of white adipose tissue encoding for F4/80, Mac-1, Mac-2, CD11c, MCP-1, TNF-α, and IL-6 were determined by using whole white adipose tissue RNA isolated by RNeasy columns (Qiagen) and analyzed as described above.

Western Blot Analysis. Livers were homogenized in protein lysis buffer, and Western blot procedures were performed as previously described. Antibodies used in this study are: NEMO (R. Gareus, personal communication) (IMG-324A, Imgenex), Akt (#9272, Cell signaling), IKK-1 (#1615–1 Epitomics), IKK-2 (#2370, Cell Signaling), P-AKT (#9271, Cell Signaling), and P-STAT-3 (sc-8059, Santa Cruz Biotechnology).

Immunohistochemistry. Livers were either frozen in tissue-freezing medium (Jung Tissue Freezing Medium, Leica Microsystems) and sectioned on a cryostat or fixed in 4% paraformaldehyde following a protocol as described (10). Sections were either stained with H&E, TUNEL (Promega), anti-Ki-67 antibody (sc-7846, Santa Cruz Biotechnology), anti-F4/80 antibody (MCAP-497, Serotec), or Sudan (Acros Organics).

Statistical Analyses. Datasets were analyzed for statistical significance by using a two-tailed, unpaired Student's *t* test. *P* values <0.05 were considered significant.

ACKNOWLEDGMENTS. We thank Brigitte Hampel, Sigrid Irlenbusch, and Julian Zotz for excellent technical help. Nemo antibody was a gift from Ralph Gareus (Institute for Genetics, University of Cologne, Cologne, Germany). This work was supported by the Centre for Molecular Medicine Cologne.

1. Hotamisligil GS, Shargill NS, Spiegelman BM (1993) *Science* 259:87–91.
2. Xu H, Barnes GT, Yang Q, Tan G, Yang D, Chou CJ, Sole J, Nichols A, Ross JS, Tartaglia LA, Chen H (2003) *J Clin Invest* 112:1821–1830.
3. Plomgaard P, Bouzakri K, Krogh-Madsen R, Mittendorfer B, Zierath JR, Pedersen BK (2005) *Diabetes* 54:2939–2945.
4. Hotamisligil GS, Arner P, Caro JF, Atkinson RL, Spiegelman BM (1995) *J Clin Invest* 95:2409–2415.
5. Hotamisligil GS, Peraldi P, Budavari A, Ellis R, White MF, Spiegelman BM (1996) *Science* 271:665–668.
6. Tuncman G, Hirosumi J, Solinas G, Chang L, Karin M, Hotamisligil GS (2006) *Proc Natl Acad Sci USA* 103:10741–10746.
7. Hirosumi J, Tuncman G, Chang L, Gorgun CZ, Uysal KT, Maeda K, Karin M, Hotamisligil GS (2002) *Nature* 420:333–336.
8. Cai D, Yuan M, Frantz DF, Melendez PA, Hansen L, Lee J, Shoelson SE (2005) *Nat Med* 11:183–190.
9. McTiernan A (2005) *Oncology* 19:871–881; discussion 881–882, 885–886.
10. Yoshioka Y, Hashimoto E, Yatsuji S, Kaneda H, Taniai M, Tokushige K, Shiratori K (2004) *J Gastroenterol* 39:1215–1218.
11. Maeda S, Kamata H, Luo JL, Leffert H, Karin M (2005) *Cell* 121:977–990.
12. Pikarsky E, Porat RM, Stein I, Abramovitch R, Amit S, Kasem S, Gutkovich-Pyest E, Urieli-Shoval S, Galun E, Ben-Neriah Y (2004) *Nature* 431:461–466.
13. Luedde T, Beraza N, Kotsikoris V, van Loo G, Nenci A, De Vos R, Roskams T, Trautwein C, Pasparakis M (2007) *Cancer Cell* 11:119–132.
14. Schmidt-Supprian M, Bloch W, Courtois G, Addicks K, Israel A, Rajewsky K, Pasparakis M (2000) *Mol Cell* 5:918–992.
15. Kellendonk C, Opherk C, Anlag K, Schutz G, Tronche F (2000) *Genesis* 26:151–153.
16. Inoue M, Ohtake T, Motomura W, Takahashi N, Hosoki Y, Miyoshi S, Suzuki Y, Saito H, Kohgo Y, Okumura T (2005) *Biochem Biophys Res Commun* 336:215–222.
17. Keller H, Dreyer C, Medin J, Mahfoudi A, Ozato K, Wahli W (1993) *Proc Natl Acad Sci USA* 90:2160–2164.
18. Herzig S, Hedrick S, Morantte I, Koo SH, Galimi F, Montminy M (2003) *Nature* 426:190–193.
19. Shimano H, Yahagi N, Amemiya-Kudo M, Hasty AH, Osuga J, Tamura Y, Shionoiri F, Iizuka Y, Ohashi K, Harada K, *et al*. (1999) *J Biol Chem* 274:35832–35839.
20. Patsouris D, Reddy JK, Muller M, Kersten S (2006) *Endocrinology* 147:1508–1516.
21. Drucker C, Parzefall W, Teufelhofer O, Grusch M, Ellinger A, Schulte-Hermann R, Grasl-Kraupp B (2006) *Carcinogenesis* 27:152–161.
22. Luedde T, Assmus U, Wustefeld T, Meyer zu Vilsendorf A, Roskams T, Schmidt-Supprian M, Rajewsky K, Brenner DA, Manns MP, Pasparakis M, Trautwein C (2005) *J Clin Invest* 115:849–859.
23. Streetz KL, Luedde T, Manns MP, Trautwein C (2000) *Gut* 47:309–312.
24. Arkan MC, Hevener AL, Greten FR, Maeda S, Li ZW, Long JM, Wynshaw-Boris A, Poli G, Olefsky J, Karin M (2005) *Nat Med* 11:191–198.
25. Yuan M, Konstantopoulos N, Lee J, Hansen L, Li ZW, Karin M, Shoelson SE (2001) *Science* 293:1673–1677.
26. Schmidt-Supprian M, Courtois G, Tian J, Coyle AJ, Israel A, Rajewsky K, Pasparakis M (2003) *Immunity* 19:377–389.
27. Inoue H, Ogawa W, Ozaki M, Haga S, Matsumoto M, Furukawa K, Hashimoto N, Kido Y, Mori T, Sakaue H, *et al*. (2004) *Nat Med* 10:168–174.
28. Inoue H, Ogawa W, Asakawa A, Okamoto Y, Nishizawa A, Matsumoto M, Teshigawara K, Matsuki Y, Watanabe E, Hiramatsu R, *et al.* (2006) *Cell Metab* 3:267–275.
29. Beier K, Volkl A, Fahimi HD (1997) *FEBS Lett* 412:385–387.